Journal of Marine Research, 52, 197–217, 1994

Frictional decay of abyssal boundary currents

by Parker MacCready[1,2]

ABSTRACT

A theory is presented to explain the observed longevity of abyssal boundary currents flowing along sloping topography. Typically such currents are many Rossby radii wide, and their energy is dominantly potential, residing in the broad upturn of isopycnals near the slope. The rate of decay of energy, on the other hand, is governed by the much smaller kinetic energy of the flow absorbed by the bottom boundary layer. The spin-down time is thus increased by a (possibly large) factor of PE/KE times that required to dissipate the kinetic energy alone. The ratio PE/KE is calculated from data on two sections across the Deep Western Boundary Current in the North Atlantic, and is found to be 10 and 41 in those instances, consistent with the slow spin-down of the current in that region. The change in cross-sectional shape of the current during spin-down is predicted using a 1½-layer model. It is found that the upper tip of the current moves down the slope with a self-preserving shape, while the lower edge becomes thicker and broader. The along-slope transport of the current remains constant, even as the energy decreases. The spin-down time may be interpreted as that required for the Ekman transport to drain away the isopycnal displacement which defines the flow.

1. Introduction

The great length of the Deep Western Boundary Current (DWBC) in the North Atlantic presents an intriguing puzzle to those interested in frictional spin-down. During the long transit from its headwaters near the Denmark Strait and Faroe Bank Channel, around Greenland, and on to Newfoundland, the current is strongly bottom trapped, and is thought to experience little entrainment with overlying water. Despite the fact that the DWBC here is extremely thin and wide, typical scales being 100 km in the horizontal and 500 m vertical, and lies hard upon the continental slope, it appears to be little affected by friction. Over the entire 4000 km length of interest, the current descends less than 1000 m, and has mean velocities in excess of 0.1 m s^{-1} where current meter records are available.

It is suggested below that the behavior of the DWBC is consistent with our notions of oceanic spin-down. Most of the energy of the flow resides in the potential energy of uptilted isopycnals, while dissipation of that energy is controlled by the relatively

1. Rosenstiel School of Marine and Atmospheric Science, University of Miami, 4600 Rickenbacker Causeway, Miami, Florida, 33149, U.S.A.

2. Present address: School of Oceanography WB-10, University of Washington, Seattle, Washington, 98195, U.S.A.

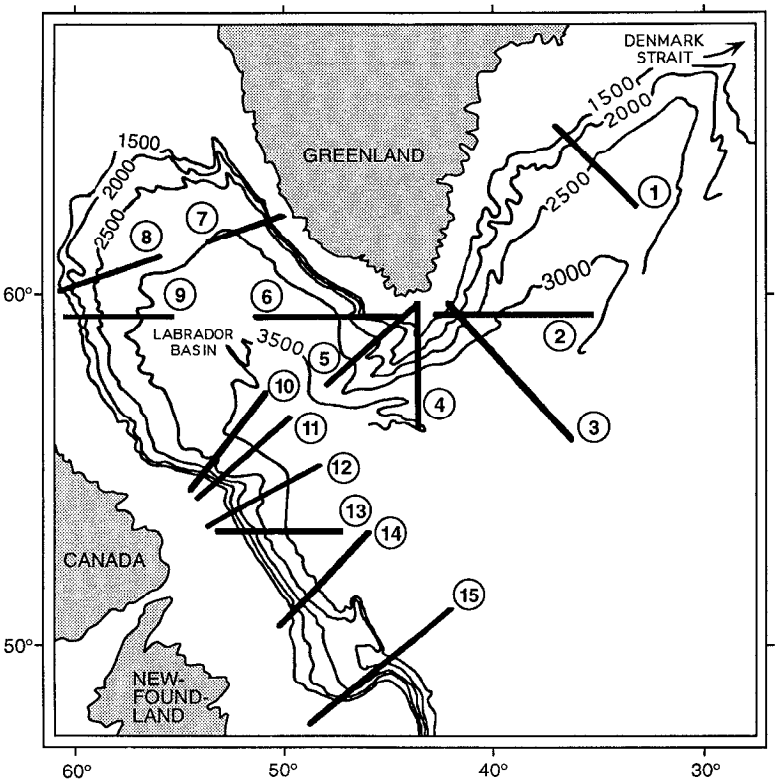

Figure 1. Bathymetry map of the region over which the DWBC flows in the northern North Atlantic, depth shown in meters. The locations of the fifteen sections presented in Figure 2 are indicated with heavy lines. The current has a source at the Denmark Strait, and is joined by water from the Faroe Bank Channel before reaching Section 1. After that the current typically flows between the 1500 m and 3500 m isobaths, winding around Greenland, and on south to Newfoundland.

small kinetic energy of the flow, as is common for currents much wider than the Rossby radius of deformation. The result is that spin-down is much longer than the time required to dissipate the kinetic energy alone.

Figure 1 shows the region of our analysis. We ignore the DWBC close to the Denmark Strait, because it entrains strongly there, and also joins with water from the Faroe Bank Channel. Barringer and Price (1990) indicate that, for overflows in general, the majority of entrainment with overlying waters occurs close to the overflow sill, typically in the first region of steeply sloping topography the current encounters, and is largely negligible thereafter. Figure 2 shows temperature contours from the 15 sections indicated in Figure 1, all presumed to be downstream of the region of strong entrainment. Isotherms are very close to isopycnals for this flow, since salinity gradients in the deep northwest Atlantic represent a relatively small

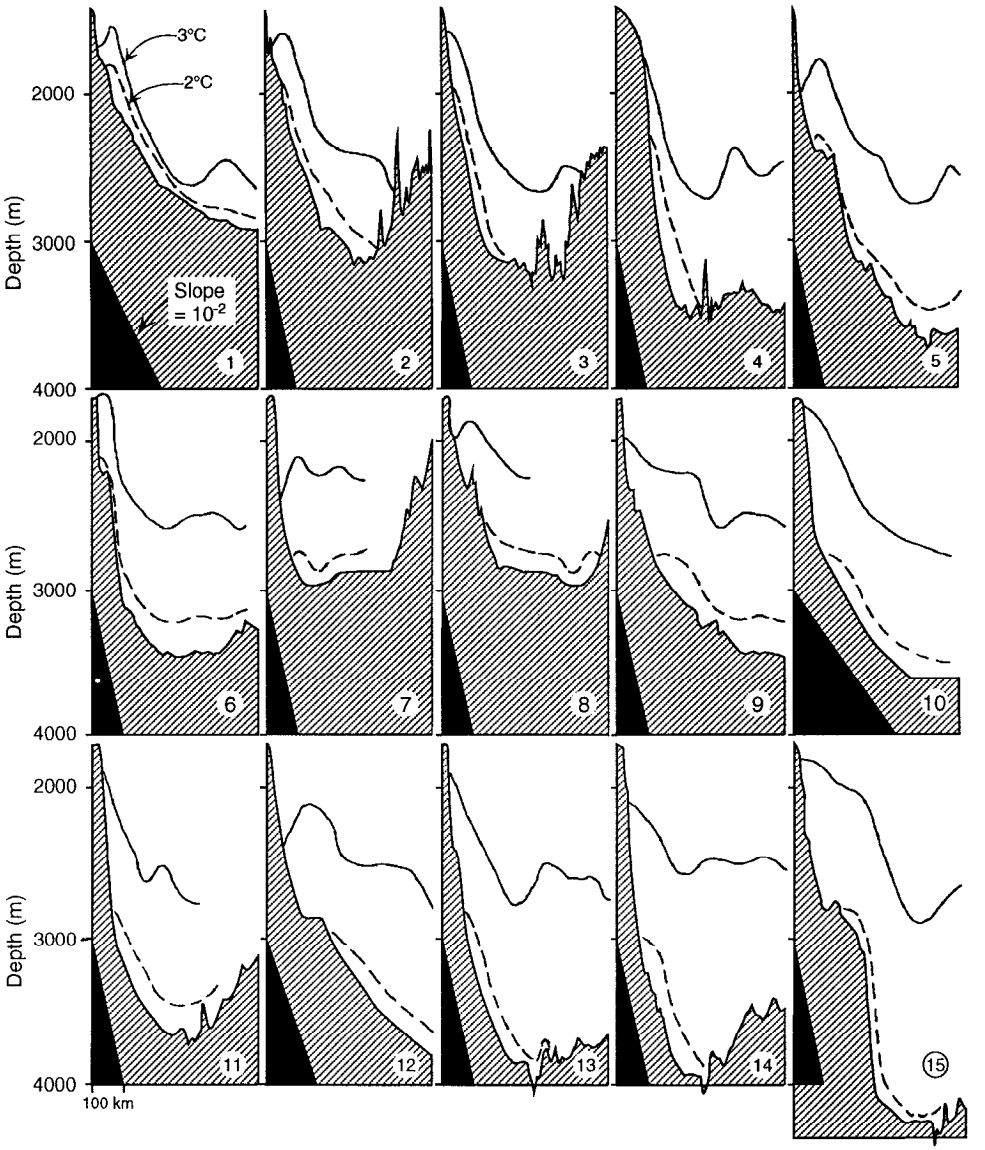

Figure 2. Isotherms in the DWBC (3°C shown with a solid line, and 2°C shown dashed) on the fifteen sections indicated in Figure 1. The sections are all from the Erika Dan atlas (Worthington and Wright, 1970) except Section 1 from Dickson *et al.* (1990), Section 10 from Lazier and Wright (1993), and Section 12 from Wallace and Lazier (1988). The triangle in the lower left of each panel indicates a slope of 10^{-2}, typical of the topography on which the DWBC rides. The lower side of each triangle is 100 km. Between Sections 1 and 15 the 2° isotherm drops roughly 1000 m, and the 3° isotherm drops a few hundred meters. The 3° isotherm appears to join the interior around 2500 m, except in Sections 7 and 8 where the flow is banked up to the north as it rounds the top of the Labrador Basin.

contribution to density. Whether or not there is substantial entrainment is in some question: the thickness between the 2° and 3° isotherms increases substantially, particularly between Sections 1 and 7. McCartney (1992) suggests that Labrador Sea Water may be entrained near section 1 as the current descends.

We limit our analysis to the region before the current rounds Flemish Cap, east of Newfoundland, where it may begin to encounter fluid of similar density (Hogg, 1983) but not of Arctic origin, confusing its identity as a gravity-driven boundary current. Even over this region, it is not clear that the current is mainly driven by its initial potential energy. It may also consist partly of a barotropic, wind-driven, Sverdrup flow (Lazier and Wright, 1993). On the other hand, it may be the return flow for the Stommel and Arons circulation driven by upwelling of deep water below the thermocline (Stommel and Arons, 1960). In a recent study by Pickart (1992) of several sections of the DWBC south of Flemish Cap, it is found that the depth of the velocity maximum actually *decreases* as one progresses downstream, indicating the possibility of some driving mechanism other than the dense source waters. Indeed, farther downstream, the DWBC evolves into something very different from a bottom-intensified flow and, by 26.5N (Leaman and Harris, 1990), the current maximum is far from the boundary. At many places along its length it has also been shown that "recirculation gyres" may strongly augment the local transport (McCartney, 1992). These issues are far from being resolved in our understanding. Below we limit our attention to the spin-down of boundary currents in which the greatest geostrophic velocity occurs just above the bottom boundary layer, a situation consistent with a flow driven by a source of dense water on a sloping boundary. These energy dissipation concepts will apply to any wide, bottom-trapped current on a slope, regardless of its ultimate energy source. In Section 2, we consider some bulk arguments about the energetics of boundary current spin-down. In Section 3, those arguments are evaluated in the light of oceanic data.

We may also analyze the specific cross-sectional shape of the current. In its initial identity as an overflow, treated by Smith (1975, 1977), the defining isopycnal of the current reconnects with the boundary at its lower edge, and has the possibility for baroclinic instability there. If instead, as we consider below, the isopycnal joins the interior stratification, the flow is more stable, and the interior provides a useful zero potential energy surface.

Stommel and Arons (1972), hereafter referred to as SA, first considered deep boundary current on a slope adjoining an interior water mass using a frictionless, 1½-layer mathematical model to explore the question of why deep boundary currents are often many times wider than the local internal Rossby radius. They assumed a current created by a source of constant potential vorticity water which adjusts into a steady boundary current on the slope, supported by a motionless body of interior water (Fig. 3). They find that while regions of interface curvature at the "tip" and "trough" are one Rossby radius wide, the region between them is not so constrained

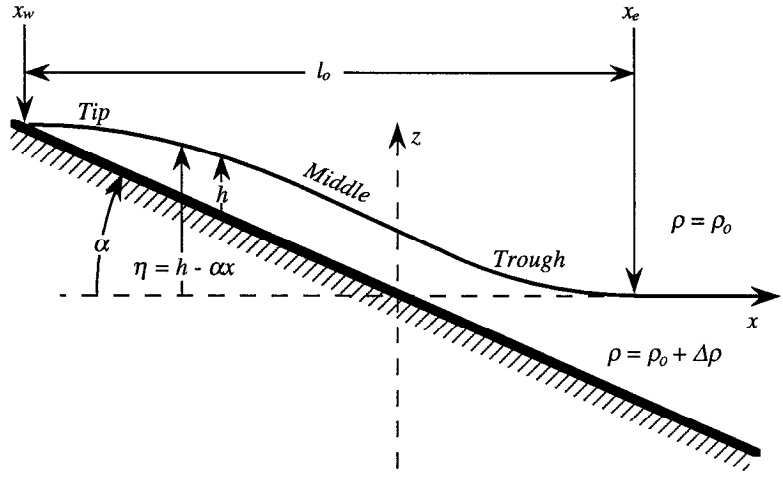

Figure 3. Definition sketch for the 1½-layer spin-down problem. The interface between heavy and light fluid is flat in the motionless interior and rises up near the slope to form the boundary current. The upper fluid of density ρ_o is taken to be infinitely deep, and motionless. The current itself is divided conceptually into three regions, the "tip," the broad "middle" over which the thickness h is nearly constant, and the "trough" where the velocity decreases to zero as it joins the interior. The positive y-axis is into the page. The slope angle α is positive as drawn, and the along-slope velocity v is negative (directed out of the page) for the current shown.

by the dynamics, and may be much wider. The current thickness in the middle is set by the initial potential vorticity, and its velocity is set by the slope angle. For the small slopes typical of the ocean the only way the current may then accommodate a large transport is by being relatively wide. Their model is extended in Section 4 to include bottom friction.

2. Energetics of spin-down

The spin-down theory relevant to the problem is provided by Gill (1981, 1982), Garrett and Loder (1981), and Garrett (1982), who derive general expressions for the energetics of baroclinic, quasi-geostrophic flow. For a baroclinic ocean current of thickness H which spins down by contact with a boundary, we may integrate the full energy equation through the thickness of the flow to show:

$$\frac{\partial}{\partial t}\int_0^H dz \left(\frac{KE + PE}{\text{unit volume}}\right) = \frac{\text{dissipation in the boundary layer}}{\text{unit area}}. \qquad (2.1)$$

The boundary layer dissipation is equal to the rate of working by the Ekman transport down the pressure gradient or, equivalently, by the current velocity times the boundary stress. This rate of pressure work in the boundary layer is given by $[\rho_o f v][-C_d|v|vf^{-1}]$ using a velocity-squared drag law (4.7, below), and ρ_o is the

reference density, f the Coriolis frequency (assumed constant; see Johnson (1993) for a treatment of the inviscid problem on a β-plane), and v the geostrophic current (assumed to be only in the y direction) above a boundary layer with drag coefficient C_d. The first term in brackets is equal to the pressure gradient in x maintaining v, while the second term in brackets is the Ekman transport in the x-direction.

The kinetic energy of the flow (per unit horizontal area) is given by $0.5\ \rho_o v^2 H$ (assuming v = const. over H) so the spin-down time, τ, may be approximated as:

$$\tau \cong \frac{H}{2C_d V}\left[1 + \frac{PE}{KE}\right], \tag{2.2}$$

where we have linearized about a flow of magnitude V. This is the spin-down time for the *energy;* the velocity and pressure fields will generally spin-down in twice this time. The relation between the density and velocity fields for flows in geostrophic balance allows us to compute the ratio KE/PE. For baroclinic, quasi-geostrophic flows of horizontal length scale L that ratio is given by $(NH/fL)^2$, which is also (internal Rossby radius/horizontal length scale)^2 for a flow with constant background buoyancy frequency N. If a flow is wide compared to the internal Rossby radius, and hence dominated by its potential energy, the spin-down time is then given approximately by

$$\tau \cong \frac{H}{2C_d V}\left(\frac{fL}{NH}\right)^2, \tag{2.3}$$

which is much longer than the spin-down time for kinetic energy alone. Physically, (2.3) may be interpreted as (half) the time it would take for the Ekman transport in the bottom boundary layer to drain away the displacement of isopycnals which drives the flow. Smith (1977) also describes the spin-down of a boundary current in terms of being drained by the Ekman transport. In the case he considers, an isolated current on a slope, the Ekman transport causes the entire current to "leak" out of its lower edge as a thin sheet, eventually extinguishing the geostrophic flow.

We may use two simple thought problems to estimate the ratio KE/PE for slope currents, and then use (2.3) to estimate their spin-down time. Figure 4 shows two arrangements of isopycnals above a boundary of constant slope α. Both assume no motion in the interior, and a constant interior stratification, defined by the buoyancy frequency N. In example (a) we have nudged the isopycnals uniformly up the slope, the result being a geostrophic boundary flow of constant magnitude out of the page. In example (b) we have pulled water of one density up the slope, forming a current which grows faster higher up the slope because of the increasing density contrast. The DWBC as it exists in our region of interest looks like a combination of the two, with many isopycnals intersecting the slope in the upper part, and constant density

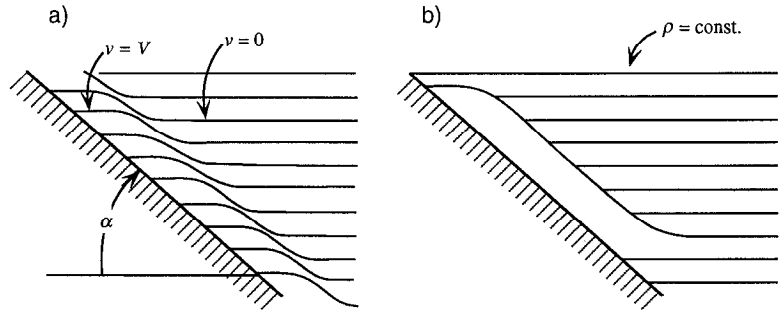

Figure 4. Two thought models of boundary currents on a slope of angle α; in both cases the current is much wider than the internal Rossby radius. In (a) we have taken the flat isopycnals of the quiescent, stratified interior and pushed them up the slope near the boundary to create a current of magnitude V there. In (b) we have placed water of a single density along the slope, allowing it to join smoothly with its interior isopycnal. In the second example the velocity in the boundary current increases as one proceeds up the slope because the density contrast increases, however the ratio of kinetic energy to potential energy remains constant.

along the slope in the lower part. For either of these cases the energies/unit volume (away from the edges of the current) may be shown to be

$$KE = \frac{1}{2}\rho_o v^2 = \frac{1}{2}\rho_o\left(\frac{g\rho'\alpha}{f\rho_o}\right)^2, \tag{2.4}$$

and

$$PE = \frac{1}{2}\rho_o\left(\frac{g\rho'}{\rho_o N}\right)^2, \tag{2.5}$$

where ρ' is the density difference between a water parcel and the interior water at that depth. Taking the ratio we find

$$\frac{KE}{PE} = \left(\frac{N\alpha}{f}\right)^2, \tag{2.6}$$

which, interestingly, is independent of the actual width of the current on the slope. Eq. (2.6) implies that H/α, the width of a horizontal slice through the current at a given depth, is the natural length scale for comparison with the internal Rossby radius, NH/f. Nevertheless, we still require that the width of the flow on the slope be much greater than NH/f since the above arguments pertain only to the broad "middle" region of the flow.

For a deep, mid-latitude ocean with $N/f \cong 10$, a boundary current of either type will be dominated by its potential energy as long as $\alpha \ll 10^{-1}$, and the "boundary

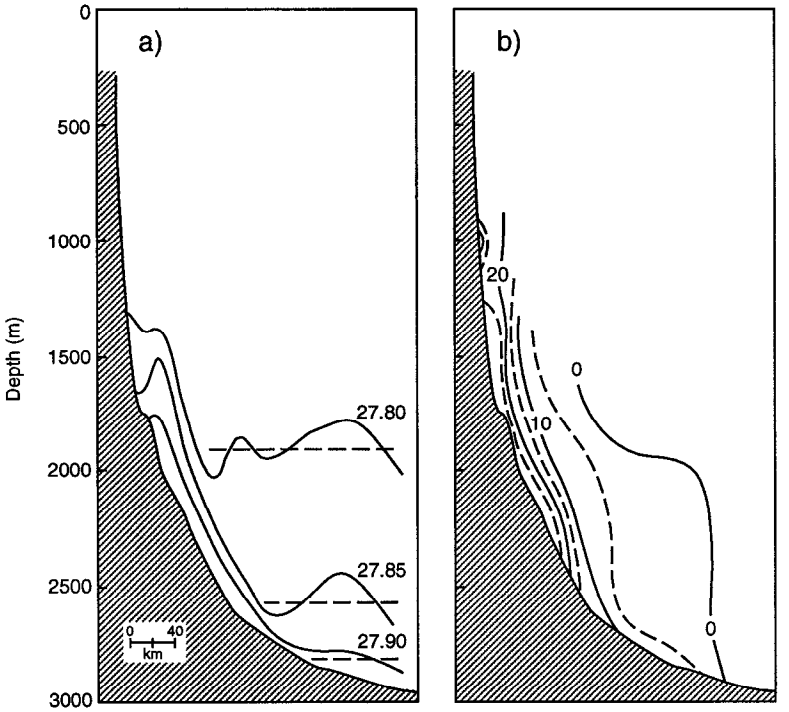

Figure 5. A close-up of Section 1, from Dickson *et al.* (1990), showing (a) σ_θ (kg m^{-3}), and (b) along-slope velocity (cm s^{-1}) out of the page. The zero-*PE* reference levels for the isopycnals (dashed lines) were: 1900 m for $\sigma_\theta = 27.80$, 2570 m for $\sigma_\theta = 27.85$, and 2820 m for $\sigma_\theta = 27.90$. The velocities are from several years of moored current meter data.

current spin-down time," τ_{bc}, will be approximately

$$\tau_{bc} \cong \frac{H}{2C_dV}\left(\frac{f}{N\alpha}\right)^2. \tag{2.7}$$

The strong dependence of (2.7) on the slope angle is important because α is the most variable of the background parameters.

A distinction between the flows in Figure 4a versus 4b is that the boundary layer physics may be drastically altered by buoyancy effects when there is a density gradient on the slope (i.e., isopycnals intersecting the slope), as in 4a. MacCready and Rhines (1993) show that Ekman transport up or down the slope gives rise to buoyancy effects which eventually arrest the Ekman transport, and with it the boundary stress, in a time of order τ_{bc}, (see also Garrett *et al.,* 1993). Such a process could be important near the upper edge of the DWBC where the stratification on the slope is equal to or greater than that of the interior (e.g., around 1600 m in Fig. 5a). The orientation of the DWBC is such that the Ekman transport is downslope, which bends isopycnals down in the boundary layer and gives rise to thick mixed layers

(Weatherly and Martin, 1978; Trowbridge and Lentz, 1991). Observations in the DWBC to date have lacked the resolution near the boundary to test the applicability of such theories, but we assume that, over the majority of its width, the DWBC has negligible density gradient on the slope, and so standard boundary layer theories will apply.

3. Spin-down time estimates for the DWBC

We may estimate the various terms in (2.7) to see if the DWBC energy is likely to be dominated by its *PE*, and what the spin-down time is. Values typical of the region are $N \cong 10^{-3}$ s^{-1}, $\alpha \cong 10^{-2}$, and $f \cong 10^{-4}$, giving a *KE*/*PE* ratio of 10^{-2}, and indicating that the spin-down will be dominated by the time required to drain away the displacement of isopycnals. This estimate is necessarily very rough though, and sensitive to errors in estimating the slope, which varies significantly over the length of the current, as well as over its width. Using different plausible values for the bottom slope in (2.6) we could have found *KE*/*PE* from 0.5×10^{-2} to 17×10^{-2}, an unacceptably broad range.

Figure 5 (from Dickson *et al.,* 1990) shows the velocity and density structure along Section 1 at the start of our region. Using this data set we may compute the energies directly, without resorting to (2.6). Dickson *et al.* give the transport, 10.7 Sv, and the mean velocity, ~ 0.27 m s^{-1}, from which we estimate the total *KE*/(unit length along current) as $\sim 1.5 \times 10^9$ J m^{-1}. To find the *PE*, we assume a reference state of zero *PE* as shown by the dashed lines in Figure 5a. When making the PE calculations, σ_2 was used instead of σ_θ and the background stratification was approximated as a linear variation between the 27.80 and 27.90 σ_θ surfaces. The *PE*/(unit length along current) is found to be $\sim 15.0 \times 10^9$ J m^{-1}, ten times the kinetic energy. A similar calculation based on data from Lazier and Wright (1993), Figure 6, yields *KE*/(unit length along current) $\sim 0.35 \times 10^9$ J m^{-1}, and *PE*/(unit length along current) $\sim 14.4 \times 10^9$ J m^{-1}, or 41 times the kinetic energy.

That the total energies of the two sections are so close is reassuring, but is probably more fortuitous than accurate. The potential energy calculation relies on a reference state which varies geographically. For example, the deepest part of the 2°C isotherm deepens nearly 1000 m between Sections 1 and 15 in Figure 2, leaving open the possibility that the current could *gain* potential energy along its path. The kinetic energy calculation for Figure 6 was made using the geostrophic velocity, referenced to 1500 dbar, which should represent the part of the current associated with the dense source water. The velocities measured by current meters are somewhat stronger in places, and could increase the kinetic energy estimate by as much as a factor of four. Lazier and Wright (1993) identify a possible barotropic, wind-driven, Sverdrup flow near the shelf break in the Labrador Sea as a likely reason for the discrepancy between current meter and geostrophic velocities. This signal is present in the current meter data in Figure 6b, particularly for the two instruments closest to

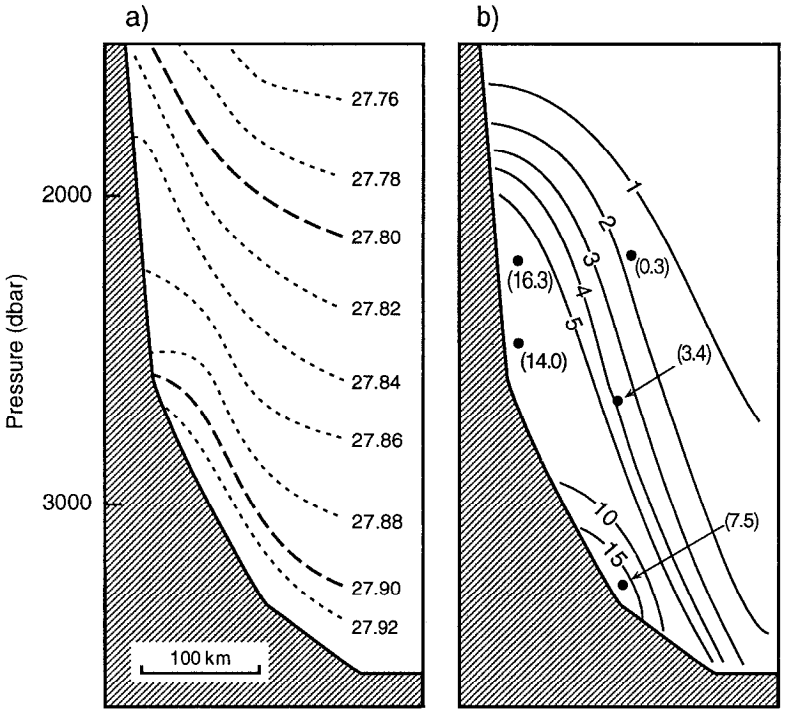

Figure 6. Isopycnals (kg m^{-3}) (a), and along-slope velocity contours (cm s^{-1}) (b), from Lazier and Wright (1993), Section 10 in Figure 1. The *PE* was calculated for $\sigma_\theta \geq 27.80$ kg m^{-3}, and the zero-*PE* reference state was taken to be approximately at the depths where the densities are listed. The isolines of velocity are given in cm s^{-1}, and are calculated geostrophically from the density in (a) using 1500 dbar as a level of no motion. The numbers in parenthesis in (b) are velocities in cm s^{-1} from year-long moored current meter records. The relatively high current meter velocities close to the slope may be due to a barotropic, wind-driven, Sverdrup flow centered on the shelf break.

the slope between 2000 and 2500 dbar. It is difficult to separate such barotropic currents out of our spin-down analysis. In fact, such currents would spin down the boundary flow more quickly, and are not accounted for in the theory presented here. Nevertheless, the ratio from the actual calculated values of *KE* and *PE* is consistent with a current dominated by its potential energy.

Having estimated the energy ratio, we turn to the other part to the spin-down time, $H\ (2C_d\ V)^{-1}$. To estimate this we use a velocity scale $V = 0.27$ m s^{-1} (probably an upper bound), $C_d = 2.5 \times 10^{-3}$, and $H = 500$ m. These give $H\ (2\ C_d\ V)^{-1} = 4.3$ days, during which time a current of 0.27 m s^{-1} would only advance 100 km. Multiplying this by an average of the observed ratios: $PE/KE = 25$, the distance is extended to 2500 km, while the total length of the DWBC from Section 1 to Section 15 is about 4000 km. Thus, the proposed theory may explain the longevity of the DWBC as a bottom trapped current, but only if PE/KE is somewhat greater than 25 over most of

the rest of its path. Unfortunately, few suitable velocity records beyond those in Figure 5 and 6 exist.

4. Details of the spin-down

Important aspects of the boundary current spin-down may be predicted analytically if we focus on a wide current over a shallow slope which has no along-slope variation. This two-dimensional current will then be allowed to spin down in time under the influence of a linearized bottom friction. Thus, for the sake of finding a solution, we will use time-dependence as a substitute for the along-slope variability of a steady current, acknowledging in advance that there are fundamental differences.[3] An important aspect of the steady current which evolves downstream is that it has, at any section across the current, a constant downstream volume transport, as long as there is no entrainment. This should be true because the current must everywhere along its length be able to carry whatever the source continually supplies. Later in this section we demonstrate that the time-dependent solution also has constant transport.

The equations of motion for the lower layer of a 1½-layer system may be written as

$$\frac{\partial u}{\partial t} + u\frac{\partial u}{\partial x} + v\frac{\partial u}{\partial y} - fv = -g'\frac{\partial \eta}{\partial x}, \tag{4.1}$$

$$\frac{\partial v}{\partial t} + u\frac{\partial v}{\partial x} + v\frac{\partial v}{\partial y} + fu = -g'\frac{\partial \eta}{\partial y}, \tag{4.2}$$

$$\frac{\partial h}{\partial t} + \frac{\partial (hu)}{\partial x} + \frac{\partial (hv)}{\partial y} = w_E. \tag{4.3}$$

Here u is the cross-slope velocity and v is the along-slope velocity in the lower layer (see Fig. 3). The upper layer is taken to be infinitely thick and motionless. The cross-slope and along-slope coordinates are x and y, the topography is given by $-\alpha x$, where α is the slope angle and $\alpha \ll 1$. We have assumed that the temporal and spatial Rossby numbers are small (i.e. the time-dependent and inertial terms are small compared with the Coriolis acceleration), and that the current is much wider than it is thick. This results in a vertical momentum equation which is hydrostatic to very good approximation, and allows us to express the horizontal pressure gradients in (4.1) and (4.2) in terms of the reduced gravity $g' \equiv g\,\Delta\rho/\rho_o$ and the tilt of the

3. Note, however, that in non-rotating laminar boundary layer theory, the Blasius boundary layer (steady with downstream evolution) is very similar to the boundary layer over an infinite flat plate set impulsively in motion, if time is substituted for downstream distance divided by free-stream velocity. The two solutions are functions of identical similarity variables under this substitution, and the functions are at most 50% different at any given value of the similarity variable.

Also, since we are concentrating on wide currents which have (by construction) a broad middle region of constant along-slope velocity, *most* of the fluid should move approximately the same distance under either set of assumptions.

interface η. The upper layer has density ρ_o and that of the lower layer is $\rho_o + \Delta\rho$. The two momentum equations, (4.1) and (4.2), are meant to describe only the flow in the lower layer *above the bottom boundary layer,* so dissipation is ignored except where it forces Ekman pumping and changes h through Eq. (4.3). That we ignore dissipation at the interface is a tacit acknowledgement that the shear there in the ocean is typically much weaker than that in the bottom boundary layer. Eq. (4.3) is a vertical integral of the continuity equation $\nabla \cdot \boldsymbol{u} = 0$ with the stipulation that water parcels on the upper interface remain on that interface, while those at the top of the bottom boundary layer may be moved off that surface by the Ekman pumping velocity w_E.

If we further assume there is no along-slope variation of the current ($\partial/\partial y = 0$), and that the non-linear (inertial) terms in (4.1) and (4.2) may be ignored compared with the time-dependent terms, the equations may be re-written

$$fv = g' \left(\frac{\partial h}{\partial x} - \alpha \right), \tag{4.4}$$

$$\frac{\partial v}{\partial t} + fu = 0, \tag{4.5}$$

$$\frac{\partial h}{\partial t} = \frac{2\, C_d |v|}{f} \frac{\partial v}{\partial x}, \tag{4.6}$$

where we have made use of the relation between interface height and layer thickness $\eta = h - \alpha x$ in (4.4). To this approximation, the along-slope velocity is geostrophic (z4.4) and the cross-slope velocity is the much smaller ageostrophic flow associated with temporal changes in v through (4.5). The evolution of lower layer thickness is now dominated by Ekman pumping (4.6), consistent with small cross-slope velocities. The Ekman pumping in (4.6) has been derived from a velocity-squared drag law:

$$\textbf{stress} = -\rho_o C_d (u^2 + v^2)\, (\cos\theta, \sin\theta) \tag{4.7}$$

where **stress** is the horizontal stress vector at the bottom boundary and $\theta \equiv \tan^{-1}(v/u)$. Linearizing the Ekman pumping about the along-slope velocity of magnitude V characteristic of the middle region, $V \equiv |-g'\, \alpha f^{-1}|$, we may rewrite (4.6) as

$$\frac{\partial h}{\partial t} = \frac{2\, C_d V}{f} \frac{\partial v}{\partial x}. \tag{4.8}$$

We may then combine (4.4) with (4.8) to form a governing equation for h:

$$\boxed{\frac{\partial h}{\partial t} = D \frac{\partial^2 h}{\partial x^2}}, \tag{4.9}$$

where

$$D \equiv 2\, C_d V g' f^{-2}. \tag{4.10}$$

An analogous result is given by Gill (1982, pp. 353–354) for homogeneous rotating flow when the horizontal scale is much greater than the Rossby radius of deformation. This approximation is true of our derivation as well because we assume a small spatial Rossby number to eliminate inertial terms. However, while the current may be many Rossby radii wide, regions of significant variation such as the tip and trough may not be, invalidating the approximation (and signaling the need to retain the inertial terms). This will be checked below when we have a solution in hand.

The approximations used to derive (4.9) are not uniformly valid for the situation shown in Figure 3. Near the tip, the lower layer thickness will become less than the boundary layer thickness (e.g. over the last kilometer of width for a 10 m thick boundary layer on a slope of 10^{-2}). Below we find that the tip is a rather quiet, well-behaved region which is essentially dragged along by the more correctly-approximated middle region, so this should not be a problem. The linearization of the drag law will over-estimate the drag for low velocities. Nevertheless, it gives the same general behavior as the velocity-squared drag law.

SA considered the situation shown in Figure 3 without bottom friction. Taking $C_d = 0$ in (4.6), we find that h, and hence u and v, are steady, that $u = 0$, and that v is given by (4.4). They also stipulate that all the moving fluid in the current should have the same potential vorticity, i.e.

$$\left(\frac{\partial v}{\partial x} + f\right) h^{-1} = f h_o^{-1} \tag{4.11}$$

between x_w and x_e as shown in Figure 3. For small slope angles SA find (correcting a typographical error) that

$$h = h_o + \frac{\alpha\lambda}{1 + e^{-l_o\lambda^{-1}}} \left(e^{(x-x_e)\lambda^{-1}} - e^{-(x-x_w)\lambda^{-1}}\right), \tag{4.12}$$

where $\lambda \equiv (g' h_o)^{1/2} f^{-1}$ is the internal Rossby radius, and $l_o \equiv (x_e - x_w)$. The total width of the current is then determined by the transport it is required to carry. For typical DWBC values[4], SA show that the solution is many Rossby radii wide, with a broad middle region where $h = h_o$, and rounding off over a distance λ at the tip and trough to bring v to zero (at the tip, their solution also generally calls for a region of motionless fluid which the current joins). Since the interface in the middle closely follows the slope, the velocity there is controlled by the slope angle, and the thickness by the initial potential vorticity. Hence, SA show that, to carry a large transport, the current must be very wide, consistent with observations.

The general idea from SA of a broad current with $h = h_o$ in the middle provides the starting point for a solution to the time-dependent frictional problem governed by (4.9). Because there is evolution of the thickness only where it has curvature, the

4. Using $h_o = 400$ m, $g' = 10^{-3}$ m s^{-2}, $\alpha = 10^{-2}$, $f = 10^{-4}$ s^{-1}, and an along-slope transport of -10 Sv, we find $l_o \cong$ (transport)$/(h_o V) = 250$ km, while $\lambda = 6$ km.

middle will be unchanged for some time, and we expect all variability will be at the tip and trough. This motivates us to look for separate solutions in those places, patching them onto the broad middle.

a. Tip solution. Fluid drains out of the tip region at a rate determined by the Ekman transport in the middle, which should be relatively constant for our assumptions. Thus we expect a solution where the tip maintains a constant shape which translates down-slope at a rate given by

$$U_{\text{tip}} = \frac{\text{middle Ekman transport}}{h_o} = \frac{C_d V^2}{f h_o} \tag{4.13}$$

using V as defined above to linearize the drag law. Based on this expectation, we transform the diffusion equation (4.9) to a frame of reference which moves with the tip, using

$$h(x, t) = h(\zeta), \tag{4.14}$$

where

$$\zeta \equiv (x - U_{\text{tip}} t), \tag{4.15}$$

and t is time. Eq. (4.9) becomes

$$\frac{\partial^2 h}{\partial \zeta^2} + \frac{\alpha}{h_o} \frac{\partial h}{\partial \zeta} = 0. \tag{4.16}$$

The boundary conditions are:

$$\text{(i)} \qquad h = 0 \qquad \text{for} \qquad \zeta = \zeta_o \tag{4.17}$$

$$\text{(ii)} \qquad h \to h_o \qquad \text{as} \qquad \zeta \to \infty, \tag{4.18}$$

where ζ_o is the value of ζ at $t = 0$. Boundary condition (i) says that the thickness goes to zero at a point which moves downslope at a velocity U_{tip}, while (ii) assures that the solution joins the middle smoothly. The tip solution is then:

$$h_{\text{tip}} = h_o \left[1 - \exp\left(-\frac{\alpha}{h_o} (\zeta - \zeta_o) \right) \right]. \tag{4.19}$$

Thus, the tip is rounded off over a width h_o/α instead of the scale λ from the SA solution. This is not inconsistent: the diffusive solution alters the potential vorticity of the fluid as the tip passes by on its way downslope (note that while the tip *shape* is moving down, this is not true of the *fluid,* see Section 4c). One may also see from (4.19) that the slope of the interface where $h = 0$ is exactly flat, so the velocity goes to zero there. The Ekman pumping, however, is a maximum at that point.

b. Trough solution. Intuitively, the solution in the trough will not propagate like that of the tip, a fact which thwarts any attempt at a global solution. Nevertheless we may

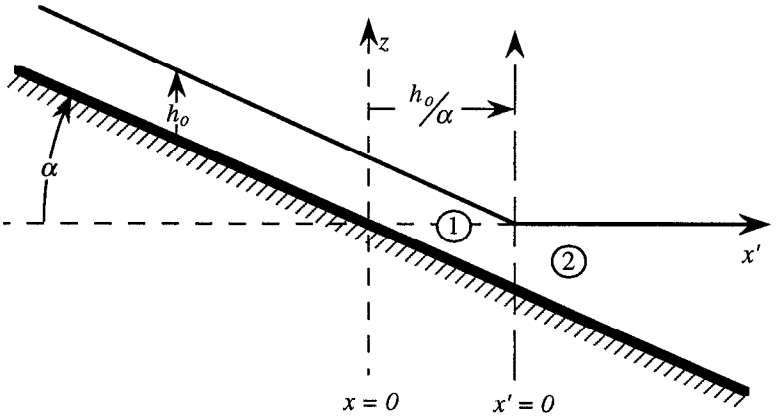

Figure 7. Definition sketch for the "trough" solution initial condition.

find a solution which applies at the trough and merges smoothly with the broad middle region (*before* the tip moves all the way down to the trough). Motivated by the different potential vorticity fields between the middle where $h = h_o$, and the interior basin to the "east" where $h = \alpha x$, we will use the somewhat arbitrary initial condition shown in Figure 7. This has a kink at $x' = 0$, where $x' \equiv x - h_o/\alpha$. Then we search for separate solutions h_1 and h_2 in regions 1 and 2 which match at $x' = 0$; also we formally change variables from x to x', which does not alter the form of the governing diffusion equation (4.9). The boundary/matching conditions are

$$\text{(i)} \qquad \frac{\partial h_1}{\partial x'} = \frac{\partial h_2}{\partial x'} \qquad \text{at} \qquad x' = 0, \tag{4.20}$$

$$\text{(ii)} \qquad \frac{\partial^2 h_1}{\partial x'^2} = \frac{\partial^2 h_2}{\partial x'^2} \qquad \text{at} \qquad x' = 0. \tag{4.21}$$

Condition (i) matches along-slope velocities, while condition (ii) matches the Ekman pumping, which also ensures (through 4.9) that the thicknesses, initially equal at $x' = 0$, remain equal for all time there. The problem then amounts to solving the diffusion equation with a flux boundary condition (see e.g. White, 1974, p. 159). The solution, valid on both sides of $x' = 0$, may be shown to be

$$h_{\text{trough}} = \frac{\alpha}{2} x' \left[1 + \text{erf}(s)\right] + \alpha \sqrt{\frac{Dt}{\pi}} e^{-s^2} + h_o \tag{4.22}$$

where $s \equiv 0.5\, x'\, (Dt)^{-1/2}$ is the usual similarity variable for diffusion problems. The slope of h_{trough} at $x' = 0$ is always $\alpha/2$, and the thickness at $x' = 0$ increases according to

$$h_{\text{trough}}(x' = 0) = h_o + \alpha \sqrt{\frac{Dt}{\pi}}. \tag{4.23}$$

c. Discussion of the time-dependent solution. During its initial evolution, the trough solution violates the assumptions used to derive the diffusion equation, since the velocity at the kink varies in x' over a distance smaller than the Rossby radius. Thus, the solution is not formally valid before a time given approximately by $2(Dt)^{1/2} \gg \lambda$, or $t \gg h_o (8 C_d V)^{-1}$. For $h_o = 400$ m, $C_d = 2.5 \times 10^{-3}$, and $V = 0.1$ m s^{-1} this time is 2.3 days, quite short compared to the many months required for the current to spin down. The tip solution is also subject to a constraint on its width in order for the non-linear terms to be negligible which may be expressed as $h_o/\alpha \gg \lambda$. For $h_o = 400$ m, $\alpha = 10^{-2}, g' = 10^{-3}$ m s^{-2}, and $f = 10^{-4}$ s^{-1}, we find $h_o/\alpha = 40$ km while $\lambda = 6.3$ km, reasonably satisfying the requirement.

Two examples of the full solution are presented in Figure 8 using the parameter values from the previous paragraph, except that in (a) $\alpha = 10^{-2}$, while in (b) $\alpha = 0.5 \times 10^{-2}$. In both cases the along-slope transport was set at -10 Sv initially and solutions are shown at $t = 0$, 0.5, 1.0, and 1.5 years. Note that the tip and trough solutions will match only as long as there is a middle region over which h is very close to h_o. As time progresses this will no longer be true: the advancing tip will try to make the middle thinner, while the widening trough will try to make it thicker. As this happens the flow should still be well-behaved but our analytic solution will no longer be valid. However, as shown in Figure 8, the solutions are useful over a long time for reasonable parameter choices.

At the initial time in the two examples in Figure 8 the current has the same vertical extent (i.e., the height of the tip above the trough), although in case (b) with shallower slope it is twice as wide and has twice the cross-sectional area. Because the velocity is decreased in (b) the two examples have the same along-slope transport.

We expect that the steady-state current which evolves in shape along its length will have a constant transport through any section. Interestingly, the time-dependent solution we have developed, which lacks y-dependence, also has constant transport even as its energy decays. To show this, consider the rate of change of transport:

$$\frac{\partial}{\partial t}(\text{transport}) = \frac{\partial}{\partial t}\int_{x_w}^{x_e} (h\,v)\,dx = \frac{\partial}{\partial t}\int_{x_w}^{x_e} \frac{g'}{f}\left(h\frac{\partial h}{\partial x} - \alpha h\right)dx, \tag{4.24}$$

where x_w is a coordinate which moves with the tip and x_e is far enough east (positive x-direction) of the current that there is no appreciable velocity there over the time of interest. Noting that $h(x = x_w) = 0$, and that $\partial x_e/\partial t = 0$, (4.24) may be reduced to

$$\frac{\partial}{\partial t}(\text{transport}) = \frac{g'}{f}\int_{x_w}^{x_e} \frac{\partial h}{\partial t}\,dx. \tag{4.25}$$

Then using the diffusion equation (4.9) to substitute $D\partial^2 h/\partial x^2$ for $\partial h/\partial t$ the integration may be carried out to show that

$$\frac{\partial}{\partial t}(\text{transport}) = \frac{-Dg'}{f}\left[\frac{\partial h}{\partial x_{(x=x_w)}} - \alpha\right]. \tag{4.26}$$

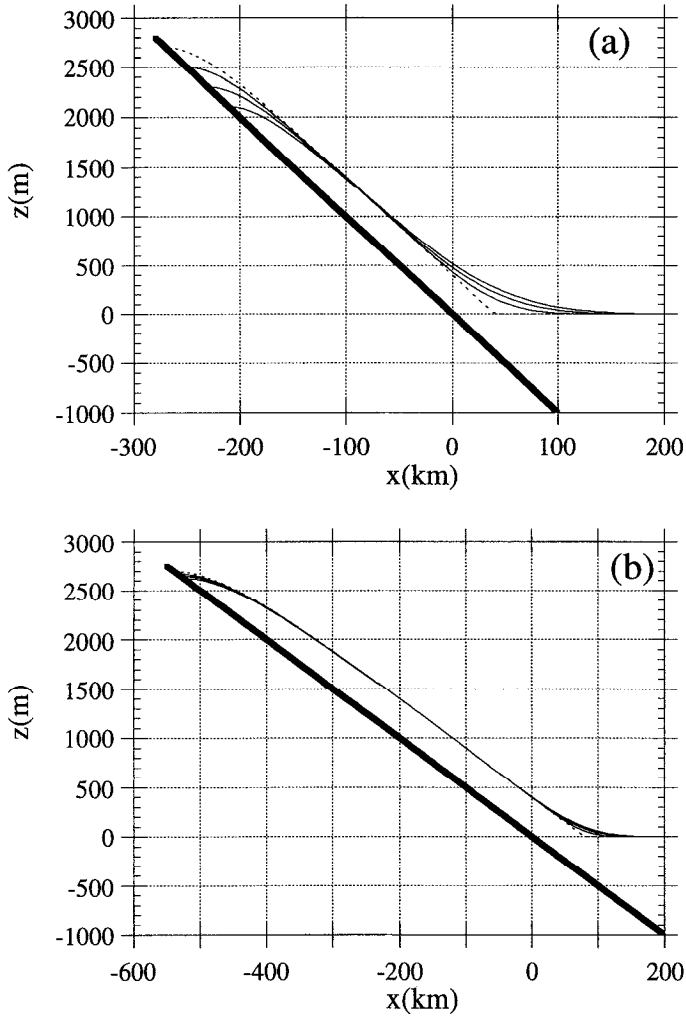

Figure 8. Examples of the analytic solution: (4.19) patched in the "middle" to (4.22), for (a) $\alpha = 10^{-2}$, and (b) $\alpha = 0.5 \times 10^{-2}$. Solutions are shown at four different times: $t = 0$ (dashed), $t = 0.5$, 1.0, and 1.5 years (solid). As time progresses, the shape-preserving tip slides downslope at a constant rate, while the trough thickens and becomes broader. For both cases $f = 10^{-4}\ \mathrm{s}^{-1}$, $g' = 10^{-3}\ \mathrm{m\ s}^{-2}$, $C_d = 2.5 \times 10^{-3}$, $h_o = 400$ m, and the initial along-slope transport is -10 Sv. In (a) $V = 0.1\ \mathrm{m\ s}^{-1}$, while in (b) $V = 0.05\ \mathrm{m\ s}^{-1}$ because of the reduced slope angle. Note that the currents have the same initial vertical extent, but that (b) is twice as wide as (a). The spin-down time increases with decreasing slope angle like α^{-3}, as evidenced by the relatively rapid draining in (a) vs. (b).

From the tip solution, $\partial h/\partial x(x = x_w) = \alpha$ (i.e. the isopycnal is flat there) and the terms on the r.h.s. of (4.26) cancel, so the transport is constant in time. Thus, the time-dependent solution retains one of the important qualities we expect of a more realistic steady solution with along-path variation.

The energy spin-down time for the analytic solution is most easily estimated as half the time required for U_{tip} to traverse the initial width of the current. Taking this initial width to be $l_o \equiv (x_e - x_w)$ at $t = 0$ the spin-down time is

$$\tau = \frac{l_o}{2\,U_{tip}} = \frac{l_o f h_o}{2\,C_d V^2}. \tag{4.27}$$

Note that l_o will vary like α^{-1}, as is evident in the two examples in Figure 8; also V will vary as α, since it is taken to be the along-slope velocity scale in the middle region. Thus τ varies strongly with slope angle, going like α^{-3}, as seen in the relatively slow change of the shallow-slope current in Figure 8(b). Since most ocean basins below the shelf-slope break have topography which is concave, i.e. a slope angle which decreases in magnitude with depth, it is likely that a current flowing along the slope would spin-down noticeably only in regions of steep slope, ending up at a place of gentler slope, where the longer spin-down time would make further sinking very slow. If the region of steep slope extends below the level of the interior isopycnals which define the boundary current, the flow may spin down more fully, losing its character as thin and boundary-trapped as the tip merges with the trough. Still, the volume transport must remain constant, so perhaps the flow would eventually look more like the DWBC farther south, where it is detached from the boundary.

We may show the energies, and their ratio, for a very wide, thin, two-layer boundary current to be:

$$\frac{KE}{\text{unit } y} = \frac{1}{2}\rho_o V^2 h_o l_o, \tag{4.28}$$

$$\frac{PE}{\text{unit } y} = \frac{1}{2}\rho_o g' \alpha\, h_o l_o^2, \tag{4.29}$$

$$\frac{KE}{PE} = \frac{V}{f l_o}. \tag{4.30}$$

Using this ratio we may rewrite the spin-down time (4.27) as:

$$\tau = \frac{h_o}{2\,C_d V}\left(\frac{PE}{KE}\right) \tag{4.31}$$

which is identical with the expression derived by our energy argument in (2.2) when $KE \ll PE$.

As the current evolves during spin-down, the along-slope velocities change in time, and from Eq. (4.5), there will be cross-slope displacements associated with these changes. Integrating (4.5) in time

$$\Delta x = -f^{-1}\,\Delta v \tag{4.32}$$

where Δx is the cross-slope displacement experienced by a water parcel consistent with a change in along-slope velocity Δv. As the tip passes a location, the velocity goes from $-g'\alpha/f$ to zero, hence $\Delta v = g'\alpha/f$ and $\Delta x = -g'\alpha/f^2$. For our typical parameter choices (as in Fig. 8a) this implies an *upslope* displacement of 1 km. That the water displacement should be upslope while the tip shape movement is downslope may seem surprising, but is consistent with the requirement that the along-slope velocity decrease to zero by Coriolis acceleration as the tip arrives. Similarly, one may show that fluid parcels at the trough are pushed away from $x' = 0$ by a maximum of 0.5 km for the above parameter values as the trough solution develops.

5. Conclusion

The spin-down of abyssal boundary currents on sloping topography has been analyzed above for the case of a wide, thin current which joins a motionless water-mass at its lower edge. Using time-evolution as a substitute for spatial variability, a simple mathematical model was developed with a diffusion equation governing changes in current thickness. An analytic solution was found where the current spun down by downslope movement of its shape-preserving tip, while the trough grew thicker and wider, spreading the region of non-zero flow. For typical DWBC values, such a current could travel many thousands of kilometers before being "drained" by Ekman pumping. Throughout its evolution, however, the along-slope transport remained constant, even as the energy decayed. The spin-down time was very sensitive to slope angle, varying as α^{-3}.

The most direct relation between theory and observed currents is through the energy ratio, *PE/KE,* which is typically large for the flows of interest. This ratio was calculated to be 10 and 41 on two sections of the DWBC where sufficient data exists. Combined with an estimate of the local rate of energy extraction by the boundary, this is probably the most reliable way to calculate the local rate of decay of an observed current. Larger integral properties, such as the rate of change of total energy between sections may not be as useful, since there are several different types of forcing which cause boundary currents, as outlined in the introduction.

Having worked out the details of an abyssal boundary current, we may question to what extent such details affect the larger patterns of the circulation. As a counter-example, consider a hypothetical Earth where a species of giant kelp grows to heights of 200 m everywhere in the abyssal ocean, drastically increasing the effective bottom boundary layer drag. Under such circumstances, our boundary current would then ooze downhill from its Arctic sources and puddle up in the northern North Atlantic instead of streaming out along the continental slope toward the equator. Such a scenario could lead to greater horizontal property gradients in the deep ocean; indeed, one of the most important effects of real abyssal boundary currents is the relatively rapid global homogenization of properties they encourage, a fact which has been of great use to the sediment studies of paleo-oceanographers. Whether the

upper ocean or climate of this alternate Earth would be changed by the abyssal circulation is a more difficult question, and one which deserves further study—not in apprehension of the appearance of our monstrous kelp, but in the spirit of wondering just how well we need to understand abyssal flows.

Acknowledgments. The author would like to thank the Rosenstiel School of Marine and Atmospheric Science at University of Miami for the fellowship which supported this research. Comments from Eric Kunze and an anonymous reviewer led to a clearer development of the ideas, particularly the solutions in Section 4. Frequent and enjoyable discussions with Claes Rooth helped in the formulation of the fundamental concepts.

REFERENCES

Barringer, M. O. and J. F. Price. 1990. A simple model of the descending Mediterranean outflow plume, *in* The Physical Oceanography of Sea Straits, L. J. Pratt, ed., Kluwer Academic Publishers, Netherlands, 537–544.

Dickson, R. R., E. M. Gmitrowicz and A. J. Watson. 1990. Deep-water renewal in the northern North Atlantic. Nature, *344,* 848–850.

Garrett, C. J. R. 1982. On spindown in the ocean interior. J. Phys. Oceanogr., *12,* 989–993.

Garrett, C. J. R. and J. W. Loder. 1981. Dynamical aspects of shallow sea fronts. Phil. Trans. Roy. Soc. London, *A302,* 563–581.

Garrett, C. J. R., P. MacCready and P. B. Rhines. 1993. Boundary mixing and arrested Ekman layers: rotating stratified flow near a sloping boundary. Annu. Rev. Fluid Mech., *25,* 291–323.

Gill, A. E. 1981. Homogeneous intrusions in a rotating stratified fluid. J. Fluid Mech., *103,* 275–295.

—— 1982. Atmosphere-Ocean Dynamics. Academic Press, 662 pp.

Hogg, N. 1983. A note on the deep circulation of the western North Atlantic: Its nature and causes. Deep-Sea Res., *30,* 945–961.

Johnson, G. C. 1993. A deep inertial jet on a sloping bottom near the equator. Deep-Sea Res., *40,* 1781–1792.

Lazier, J. R. N. and D. G. Wright. 1993. Annual velocity variations in the Labrador Current. J. Phys. Oceanogr., *23,* 659–678.

Leaman, K. D. and J. E. Harris. 1990. On the average absolute transport of the deep western boundary currents east of Abaco Island, the Bahamas. J. Phys. Oceanogr., *20,* 467–475.

MacCready, P. and P. B. Rhines. 1993. Slippery bottom boundary layers on a slope. J. Phys. Oceanogr., *23,* 5–22.

McCartney, M. S. 1992. Recirculating components to the deep boundary current of the northern North Atlantic. Prog. Oceanogr., *29,* 283–383.

Pickart, R. S. 1992. Space-time variability of the Deep Western Boundary Current oxygen core. J. Phys. Oceanogr., *22,* 1047–1061.

Smith, P. C. 1975. A streamtube model for bottom boundary currents in the ocean. Deep-Sea Res., *22,* 853–873.

—— 1977. Experiments with viscous source flows in rotating systems. Dyn. Atm. Oceans., *1,* 241–272.

Stommel, H. and A. B. Arons. 1960. On the abyssal circulation of the world ocean—II. An idealised model of the circulation pattern and amplitude in oceanic basins. Deep-Sea Res., *6,* 217–233.

—— 1972. On the abyssal circulation of the world ocean—V. The influence of bottom slope on the broadening of inertial boundary currents. Deep-Sea Res., *19,* 707–718.

Trowbridge, J. H. and S. J. Lentz. 1991. Asymmetric behavior of an oceanic boundary layer above a sloping bottom. J. Phys. Oceanogr., *21,* 1171–1185.

Wallace, D. W. R. and J. R. N. Lazier. 1988. Anthropogenic chlorofluoromethanes in newly formed Labrador Sea Water. Nature, *332,* 61–63.

Weatherly, G. L. and P. J. Martin. 1978. On the structure and dynamics of the oceanic bottom boundary layer. J. Phys. Oceanogr., *8,* 557–570.

White, F. M. 1974. Viscous Fluid Flows, McGraw Hill, New York, 725 pp.

Worthington, L. V. and W. R. Wright. 1970. North Atlantic Ocean Atlas of Potential Temperature and Salinity in the Deep Water including Temperature, Salinity, and Oxygen Profiles from the Erika Dan Cruise of 1962. Woods Hole Oceanographic Institution Atlas Series 2.

Received: *27 October, 1992;* revised: *29 November, 1993.*